Evidence for elevated and spatially variable geothermal flux beneath the West Antarctic Ice Sheet

Dustin M. Schroeder[1], Donald D. Blankenship, Duncan A. Young, and Enrica Quartini

Institute for Geophysics, University of Texas at Austin, Austin, TX 78758

Edited by Mark H. Thiemens, University of California, San Diego, La Jolla, CA, and approved May 8, 2014 (received for review March 19, 2014)

Heterogeneous hydrologic, lithologic, and geologic basal boundary conditions can exert strong control on the evolution, stability, and sea level contribution of marine ice sheets. Geothermal flux is one of the most dynamically critical ice sheet boundary conditions but is extremely difficult to constrain at the scale required to understand and predict the behavior of rapidly changing glaciers. This lack of observational constraint on geothermal flux is particularly problematic for the glacier catchments of the West Antarctic Ice Sheet within the low topography of the West Antarctic Rift System where geothermal fluxes are expected to be high, heterogeneous, and possibly transient. We use airborne radar sounding data with a subglacial water routing model to estimate the distribution of basal melting and geothermal flux beneath Thwaites Glacier, West Antarctica. We show that the Thwaites Glacier catchment has a minimum average geothermal flux of ∼114 ± 10 mW/m^2 with areas of high flux exceeding 200 mW/m^2 consistent with hypothesized rift-associated magmatic migration and volcanism. These areas of highest geothermal flux include the westernmost tributary of Thwaites Glacier adjacent to the subaerial Mount Takahe volcano and the upper reaches of the central tributary near the West Antarctic Ice Sheet Divide ice core drilling site.

subglacial hydrology | ice-penetrating radar

Heterogeneous geothermal flux and subglacial volcanism have the potential to modulate ice sheet behavior and stability by providing a large, variable supply of meltwater to the subglacial water system, lubricating and accelerating the overlying ice (1, 2). However, the magnitude and spatial pattern of geothermal flux are extremely difficult to measure, and the catchment-scale constraints derived from seismic tomography (3) and satellite magnetometry (4) produce contradicting spatial patterns and cannot resolve geothermal features relevant to local ice sheet forcing. Despite strong evidence for magma migration (5) and volcanism (5–8) beneath the West Antarctic Ice Sheet (WAIS), the limitations of these heterogeneous estimates have led modeling studies to assume unrealistic spatially uniform geothermal flux distributions (9, 10). Accurate modeling of ice sheet contributions to sea level, site selection for ice core drilling, and enhanced understanding of ice–mantle interactions all require more accurate higher-resolution estimates of the spatial distribution of geothermal flux across critical glacier catchments than are currently available.

Thwaites Glacier is one of the largest, most rapidly changing glaciers on Earth, and its landward sloping bed reaches into the deep interior of the WAIS, making it a leading component in scenarios for rapid deglaciation (9, 11). In addition, the catchment of Thwaites Glacier (Fig. 1*A*) also lies within the West Antarctic Rift System, a potentially reactivated intracontinental extension zone of low topography where crustal thinning from distributed Cretaceous and narrow-mode Cenozoic rifting produces elevated geothermal flux (5, 6, 8, 14–17). Given the setting and configuration of its catchment, heterogeneous geothermal flux beneath Thwaites Glacier is likely a significant factor in local, regional, and continental-scale ice sheet stability. Thwaites Glacier has been observed by a catchment-wide airborne radar sounding survey (11). To date, the use of radar sounding data to constrain melt rates has been limited to the interpretation of bed echo strengths (6, 18) to infer basal water or radar layer drawdown to infer melted ice loss at the bed (19). However, the interpretation of layer drawdown relies on the existence, persistence, and interpretability of layers in radar sounding profiles as well as constrained accumulation rates (19). Further, the strength of bed echoes is affected by a combination of the material and geometric properties of the ice sheet and bed which introduce ambiguities in quantitative echo interpretation (18, 20–22). Fortunately, the upstream portion of Thwaites Glacier is known to be underlain by a well-quantified subglacial water system of distributed canals (23). Distributed canals have relatively constant average depths (24), and their reflecting interfaces can be modeled as flat plates (23, 25). Therefore, geometrically corrected (18) relative bed echo strengths in the upstream region of Thwaites Glacier will be proportional to the areal coverage (25) and local flux of subglacial water. This specific knowledge of the subglacial interface can be used to overcome the limitations of radar bed echo interpretation and unambiguously establish meltwater quantities with well-bounded uncertainties.

Methods

In this analysis, we determine the mean and confidence interval uncertainties for englacial attenuation rates (26) [for both scattering and reflecting spreading geometries (18)] to produce maps of the mean (Fig. 2*A*) and range (Fig. 2*B*) of observed relative bed echo strengths. Because distributed water is in pressure equilibrium with the overlying ice, its routing will be determined by the subglacial hydrologic potential, calculated using radar-derived ice thickness and surface slope (12, 13) (Fig. 1*B*). We generate a collection of water routing models by adding noise (at the

Significance

Thwaites Glacier is one of the West Antarctica's most prominent, rapidly evolving, and potentially unstable contributors to global sea level rise. Uncertainty in the amount and spatial pattern of geothermal flux and melting beneath this glacier is a major limitation in predicting its future behavior and sea level contribution. In this paper, a combination of radar sounding and subglacial water routing is used to show that large areas at the base of Thwaites Glacier are actively melting in response to geothermal flux consistent with rift-associated magma migration and volcanism. This supports the hypothesis that heterogeneous geothermal flux and local magmatic processes could be critical factors in determining the future behavior of the West Antarctic Ice Sheet.

Author contributions: D.M.S. designed research; D.M.S. performed research; D.M.S. contributed new reagents/analytic tools; D.M.S., D.D.B., D.A.Y., and E.Q. analyzed data; and D.M.S., D.D.B., D.A.Y., and E.Q. wrote the paper.

The authors declare no conflict of interest.

This article is a PNAS Direct Submission.

Freely available online through the PNAS open access option.

[1]To whom correspondence should be addressed. E-mail: dustin.m.schroeder@utexas.edu.

This article contains supporting information online at www.pnas.org/lookup/suppl/doi:10.1073/pnas.1405184111/-/DCSupplemental.

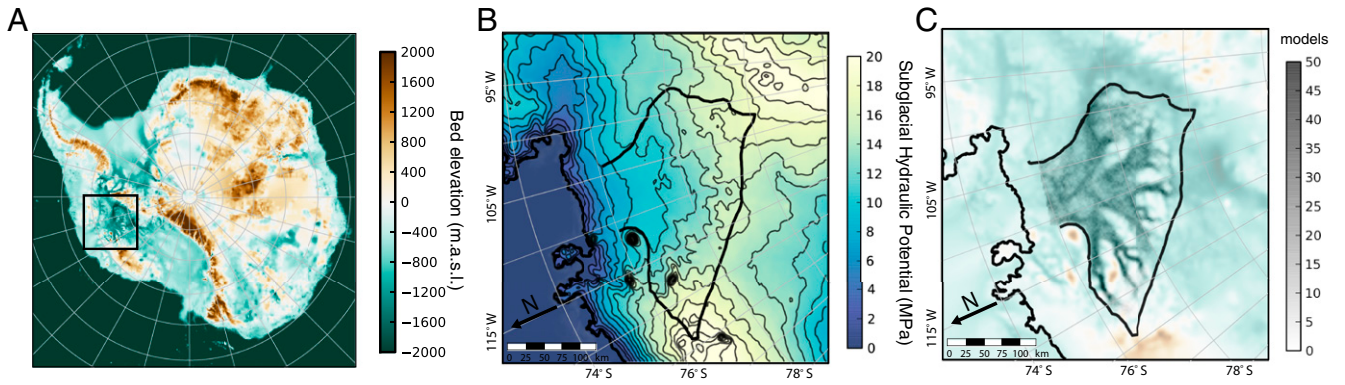

Fig. 1. Subglacial hydrologic setting of Thwaites Glacier. (*A*) Bed topography of the West Antarctic Ice Sheet and Amundsen Sea Embayment (12). (*B*) Subglacial hydrologic potential (13) for a distributed water system in the upstream region of the Thwaites Glacier catchment (black boundary). (*C*) Collection of subglacial water routing models that best fit the observed radar bed echo strength distribution (Fig. 2*A*), where the darkness of grayscale cells is the number of models (out of 50) for which these cells drain at least 10 others upstream.

scale of gridding uncertainties) to the bed topography and selecting those routes that best fit the relative bed echo strengths using uniform melt (Fig. 1*C*). We use these routing models to determine the spatial distribution of melt required to reproduce the pattern of relative echo strengths (Fig. 2*A*). We then scale the relative melt distribution by the spatial average and variance of routed subglacial water (13, 27) using the total melt from an ice sheet model of the Thwaites Glacier catchment (9). This ice sheet model includes frictional heating, horizontal advection, and an assumed uniform geothermal flux (9). Finally, we subtract the net effect of friction and advection to estimate the geothermal flux required to produce the remaining melt (Fig. 3). Details are given in *SI Methods*.

Results

The upstream region of the Thwaites Glacier catchment contains several areas of strong relative bed echoes (Fig. 2*A*) that exceed the mean bed echo strength by significantly more than the uncertainty in those strengths (Fig. 2*B*). Because the water system in this portion of the catchment is composed of distributed canals (23), high echo strengths can be interpreted as indicating larger quantities of subglacial water. The relative basal melt distribution required to fit the observed bed echo strengths with subglacial water routing models shows that water routing explains some of the strong reflections (and inferred high water quantities) in the trunk. The distribution of melt and geothermal flux (Fig. 3) includes several regions with high melt that are closely related to rift structure and associated volcanism (7, 8). These include the entire westernmost tributary (Fig. 3, location C) that flanks Mount Takahe (Fig. 3, location A), a subaerial volcano active in the Quaternary (28, 29), and several high-flux areas across the catchment adjacent to topographic features that are hypothesized to be volcanic in origin (7, 8) (e.g., Fig. 3, locations D and E). We also observe high geothermal flux in the upper reaches of the central tributaries that are relatively close to the site of the WAIS Divide ice core (Fig. 3, location B), where unexpectedly high melt and geothermal flux have been estimated.* We estimate a minimum average geothermal flux value of about 114 mW/m^2 with a notional uncertainty of about 10 mW/m^2 for the Thwaites Glacier catchment with areas exceeding 200 mW/m^2 (Fig. 3). These values are likely underestimates due to the low uniform geothermal flux value used in the ice sheet model (9) and the compensating effect of enhanced vertical advection of cold shallow ice in high-melt areas. Note that this latter effect also predicts a subtle gradient of underestimated flux from the interior to the trunk as fast flow and associated frictional melting increases.

*Clow GD, Cuffey K, Waddington E, American Geophysical Union Fall Meeting, December 3–7, 2012, abstr C31A-0577.

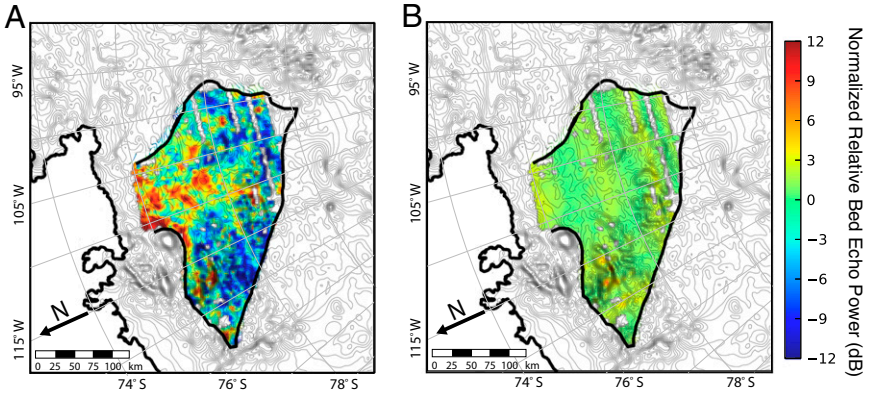

Fig. 2. Radar sounding bed echo strengths. (*A*) Mean estimate of observed relative radar bed echo strengths for the Thwaites Glacier catchment (black boundary) corrected for geometric spreading losses. (*B*) Range of estimates of corrected relative bed echo strengths. Minor banding is due to variations in aircraft height above the ice surface combined with the different geometric loss terms. Bed topography (12) contour interval for Antarctica is 180 m.

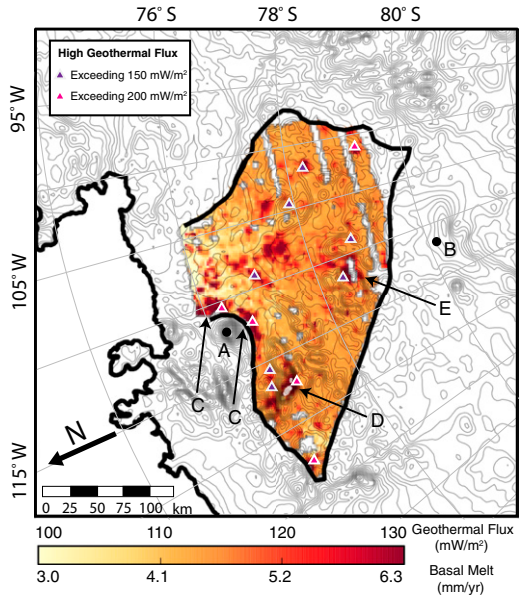

Fig. 3. Minimum geothermal flux and basal melt values required to reproduce the observed relative bed echo strengths (Fig. 2*A*) with subglacial water routing models (13, 27) (Fig. 1*C*) using the total melt water from an ice sheet model for the upstream portion of the Thwaites Glacier catchment (9). The minimum average inferred flux is ~114 ± 10 mW/m^2. High-flux areas exceed 200 mW/m^2. A indicates the Mount Takahe volcano. B indicates the WAIS Divide ice core drilling site. High-melt areas are indicated by C in the westernmost tributary, D adjacent to the Crary mountains, and E in the upper portion of the central tributaries (8). Triangles show areas where radar-inferred melt anomalies exceed those generated by ice dynamics (friction and advection) (9) and inferred geothermal flux exceeds 150 mW/m^2 (dark magenta) and 200 mW/m^2 (light magenta). Bed topography (12) contour interval for Antarctica is 180 m.

Discussion

Above, we use radar echo strengths to constrain a subglacial water routing model to estimate the pattern of basal melting and geothermal flux for the Thwaites Glacier catchment within the WAIS. The simplifying assumptions in this analysis are rooted in specific knowledge of the geometry of the subglacial water system in this area (23) and conservative treatment of radar echo strength uncertainties. Our results produce high melt values adjacent to known volcanoes and structures that are morphologically suggestive of volcanic origin (7, 8). We believe that both the magnitude and spatial pattern of geothermal flux we present reflect the geologic and glaciological reality of the Thwaites Glacier bed and that contrary to previous modeling (9), our results show regions of high geothermal flux that are in substantial agreement with levels inferred from the ice core drilling site near the ice divide for the Thwaites catchment.* This new approach provides both higher resolution and more geologically realistic boundary conditions for ice sheet modeling than previous estimates from remote sensing techniques (3, 4). These results also demonstrate an approach that can be applied to a wide variety of radar sounders (because it requires only platform stability and not absolute calibrated echo strengths) in areas known to host distributed subglacial water systems. Our results further suggest that the subglacial water system of Thwaites Glacier may be responding to heterogeneous and temporally variable basal melting driven by the evolution of rift-associated volcanism and support the hypothesis that both heterogeneous geothermal flux (6) and local magmatic processes (5) could be critical factors in determining the future behavior of the WAIS.

ACKNOWLEDGMENTS. Radar processing assistance was provided by S. Kempf, and radar interpretation was performed by J. DeSantos, A. Jones, E. Powell, and M. Williams. We thank I. Joughin for providing his modeled basal melt water values. We thank two anonymous reviewers for their helpful comments on the manuscript. We thank the National Science Foundation (NSF) (Grants PLR-0636724, PLR-0941678, and PLR-1043761), the National Aeronautics and Space Administration (Grant NNX08AN68G), and the G. Unger Vetlesen Foundation for supporting this work. D.M.S. received support from an NSF Graduate Research Fellowship, a University of Texas Recruiting Fellowship, and the University of Texas Institute for Geophysics (UTIG) Gale White Fellowship. This is UTIG contribution 2711.

1. Vogel SW, Tulaczyk S (2006) Ice-dynamical constraints on the existence and impact of subglacial volcanism on West Antarctic ice sheet stability. *Geophys Res Lett* 33(23):L23502.
2. Schoof C (2010) Ice-sheet acceleration driven by melt supply variability. *Nature* 468(7325):803–806.
3. Shapiro NM, Ritzwoller MH (2004) Inferring surface heat flux distributions guided by a global seismic model: Particular application to Antarctica. *Earth Planet Sci Lett* 223(1-2):213–224.
4. Maule CF, Purucker ME, Olsen N, Mosegaard K (2005) Heat flux anomalies in Antarctica revealed by satellite magnetic data. *Science* 309(5733):464–467.
5. Lough AC, et al. (2013) Seismic detection of an active subglacial magmatic complex in Marie Byrd Land, Antarctica. *Nat Geosci* 6(12):1031–1035.
6. Blankenship DD, et al. (1993) Active volcanism beneath the West Antarctic ice sheet and implications for ice-sheet stability. *Nature* 361(6412):526–529.
7. Behrendt JC, Finn CA, Blankenship DD, Bell RE (1998) Aeromagnetic evidence for a volcanic caldera (?) complex beneath the divide of the West Antarctic Ice Sheet. *Geophys Res Lett* 25(23):4385–4388.
8. Behrendt JC (2013) The aeromagnetic method as a tool to identify Cenozoic magmatism in the West Antarctic Rift System beneath the West Antarctic Ice Sheet—A review; Thiel subglacial volcano as possible source of the ash layer in the WAISCORE. *Tectonophysics* 585:124–136.
9. Joughin IR, et al. (2009) Basal conditions for Pine Island and Thwaites Glaciers, West Antarctica, determined using satellite and airborne data. *J Glaciol* 55(190):245–257.
10. Larour E, Morlighem M, Seroussi H, Schiermeier J, Rignot E (2012) Ice flow sensitivity to geothermal heat flux of Pine Island Glacier, Antarctica. *J Geophys Res* 117(F4):F04023.
11. Holt JW, et al. (2006) New boundary conditions for the West Antarctic Ice Sheet: Subglacial topography of the Thwaites and Smith glacier catchments. *Geophys Res Lett* 33(9):L09502.
12. Fretwell P, et al. (2013) Bedmap2: Improved ice bed, surface and thickness datasets for Antarctica. *Cryosphere* 7:375–393.
13. Le Brocq AM, Payne AJ, Siegert MJ, Alley RB (2009) A subglacial water-flow model for West Antarctica. *J Glaciol* 55(193):879–888.
14. Blankenship DD, et al. (2001) Geologic controls on the initiation of rapid basal motion for West Antarctic ice streams: A geophysical perspective including new airborne radar sounding and laser altimetry results. *The West Antarctic Ice Sheet: Behavior and Environment*, Antarctic Research Series (Am Geophys Union, Washington, DC), Vol 77, pp 105–121.
15. Corr HF, Vaughan DG (2008) A recent volcanic eruption beneath the West Antarctic Ice Sheet. *Nat Geosci* 1(2):122–125.
16. Jordan TA, et al. (2010) Aerogravity evidence for major crustal thinning under the Pine Island Glacier region (West Antarctica). *Geol Soc Am Bull* 122(5-6):714–726.
17. Bingham RG, et al. (2012) Inland thinning of West Antarctic Ice Sheet steered along subglacial rifts. *Nature* 487(7408):468–471.
18. Peters ME, Blankenship DD, Morse DL (2005) Analysis techniques for coherent airborne radar sounding: Application to West Antarctic ice streams. *J Geophys Res* 110(B6):B06303.
19. Fahnestock M, Abdalati W, Joughin I, Brozena J, Gogineni P (2001) High geothermal heat flow, basal melt, and the origin of rapid ice flow in central Greenland. *Science* 294(5550):2338–2342.
20. MacGregor JA, et al. (2007) Modeling englacial radar attenuation at Siple Dome, West Antarctica, using ice chemistry and temperature data. *J Geophys Res* 112(F3):F03008.
21. Matsuoka K (2011) Pitfalls in radar diagnosis of ice-sheet bed conditions: Lessons from englacial attenuation models. *Geophys Res Lett* 38(L5):L05505.
22. MacGregor JA, et al. (2013) Weak bed control of the eastern shear margin of Thwaites Glacier, West Antarctica. *J Glaciol* 59(217):900–912.
23. Schroeder DM, Blankenship DD, Young DA (2013) Evidence for a water system transition beneath Thwaites Glacier, West Antarctica. *Proc Natl Acad Sci USA* 110(30):12225–12228.
24. Walder JS, Fowler A (1994) Channelized subglacial drainage over a deformable bed. *J Glaciol* 40(134):3–15.
25. Knott EF, Shaeffer JF, Tuley MT (2004) *Radar Cross Section* (SciTech, Raleigh, NC).
26. Gades AM, Raymond CF, Conway H, Jacobel RW (2000) Bed properties of Siple Dome and adjacent ice streams, West Antarctica, inferred from radio-echo sounding measurements. *J Glaciol* 46(152):88–94.
27. Holmgren P (1994) Multiple flow direction algorithms for runoff modeling in grid based elevation models: An empirical evaluation. *Hydrol Processes* 8(4):327–334.
28. Lemasurier WE, Wade FA (1968) Fumarolic activity in Marie Byrd Land, Antarctica. *Science* 162(3851):352.
29. Palais JM, Kyle PR, McIntosh WC, Seward D (1988) Magmatic and phreatomagmatic volcanic activity at Mt. Takahe, West Antarctica, based on tephra layers in the Byrd ice core and field observations at Mt. Takahe. *J Volcanol Geotherm Res* 35(4):295–317.

Supporting Information

Schroeder et al. 10.1073/pnas.1405184111

SI Methods

Subglacial Water Flux and Bed Echo Strengths. Distributed subglacial canals beneath the upstream region of Thwaites Glacier (1) will have relatively constant average depths because of the relatively uniform till grain sizes and ice surface slopes in this part of the catchment (2). In this case, the fraction of the bed covered by distributed canals will be proportional to the quantity of water flowing through that area. Therefore, the relative strength of radar returns from the subsurface will be proportional to the fraction of the bed covered by subglacial water (3) and the quantity of water flowing through the area.

Radar Echo Strengths. In this analysis, we use radar data collected with a central frequency of 60 MHz, a bandwidth of 15 MHz, a pulse length of 1 μs, a 6.4-kHz pulse repetition frequency, and peak transmitted power of 8 kW (4). We processed these data by performing a series of 320 coherent summations followed by 5 incoherent averages and gridding the resulting echo strengths in a 5×5 km grid. We use only the portion of the grid that includes the upstream part of the catchment, which is underlain by a water system of distributed subglacial canals (1). There are two primary sources of uncertainty that need to be estimated, corrected, and accounted for to map relative bed echo strengths with accompanying uncertainties. The first is geometric spreading losses due to the unknown combination of reflection and scattering produced by the geometry of the basal interface (4). The second is unknown englacial attenuation due to uncertain ice temperature and chemistry (5, 6).

Geometric Spreading Losses and Englacial Attenuation. Our goal is to provide constraints on the distribution of melt and geothermal flux based only on relative bed echo strength, bed topography, and ice surface data. We use a statistical analysis of the variation of echo strengths as a function of ice thickness to estimate the range of possible englacial attenuation rates (7). Before englacial losses can be estimated, however, correction must be made for geometric spreading γ, which scales as one over the range squared for reflecting interfaces γ_r (coherent backscatter) and one over the range to the fourth power for scattering interfaces γ_s (noncoherent backscatter) (4), given by

$$\gamma_r = \frac{1}{(h + d/\sqrt{\epsilon_r})^2}$$

and

$$\gamma_s = \frac{1}{(h + d/\sqrt{\epsilon_r})^4},$$

where h is the survey height, d is the ice thickness, and $\sqrt{\epsilon_r}$ is the index of refraction for ice (4). To be conservative, we include corrections for both cases in our analysis and calculate the mean (l_μ) and 99% confidence interval ($l^-_{99\%}$, $l^+_{99\%}$) values for the two-way englacial attenuation rates l (in dB/km) for each of the geometric spreading cases (γ_r and γ_s) (8). Using these six values, we calculate P'_μ, which is the mean of the corrected relative echo strengths, given by

$$P'_\mu = \frac{1}{6}\sum_{i=1}^{6} Z'_{P_i},$$

and P'_{range}, which is the range between the maximum and minimum corrected relative echo strengths, given by

$$P'_{\text{range}} = Z'_{P_{\max}} - Z'_{P_{\min}},$$

where

$$Z'_{P_i} = \frac{P'_i - \mu_{P'_i}}{\sigma_{P'_i}},$$

$$P'_i = P\gamma_i 10^{l_i d/10},$$

P is the raw echo power, γ_i is the geometric spreading loss, l_i is the englacial attenuation loss, $\mu_{P'_i}$ is the mean across the upstream portion of the catchment, $\sigma_{P'_i}$ is the standard deviation across the catchment, and the subscript i is the index for one of the six attenuation/geometric scenarios (the mean, upper, and lower confidence interval values for both scattering and reflection geometric spreading loss cases). These values range from 7.26 to 7.31 dB/km for reflection spreading losses and 4.69 to 4.75 dB/km for scattering spreading losses.

Subglacial Water Routing. To interpret these relative echo strengths in the context of basal water quantities and melt rates, we compare them with the water quantities predicted by a subglacial water routing model assuming a distributed water system in hydrostatic equilibrium with the overlying ice (9). In this case, the subglacial hydrologic potential Φ_h is given by

$$\Phi_h = \rho_i g s + (\rho_w - \rho_i) g d,$$

where ρ_w is the density of water, ρ_i is the density of ice, g is the acceleration due to gravity, s is the ice surface elevation, and d is the ice bed elevation.

We use surface and bed topography (also on a 5×5 km grid) (10) to solve for the subglacial hydrologic potential and route water down potential using the least cost path and multiple flow direction algorithms (11), which allow water to be routed without requiring sink-filling. The gridded bed topography and resulting hydrologic potential have uncertainties due to survey spacing and gridding artifacts that can result in the erroneous routing of subglacial water and lead to a misinterpretation of melt quantities from echo strength anomalies. To address this uncertainty, we produce 1,000 bed topography realizations by adding white noise with a rms height of 100 m (approximate value of observed bed variations within a grid cell) to the gridded topography and produce a set of water routing models that assume uniform melt. From this collection of water routing models, we selected the models that produced a relative distribution of water,

$$Z_Q = \frac{Q - \mu_Q}{\sigma_Q},$$

that most closely fits the observed relative echo strengths using the cost function Δ,

$$\Delta = \sum \left(Z_Q - Z_\mu\right)^2.$$

This process selected the 50 subglacial water routing models that best explain the observed pattern of relative bed echo

strengths by routing alone (without invoking heterogeneous basal melting).

Inferred Basal Melt Rates. Each of the 50 selected routing models were used to create an average least-squares fit (12) for the relative melt F_Z required to reproduce the observed echo strengths for each of water routing models, given by

$$Z_F = \frac{M_F - \mu_F}{\sigma_F},$$

where M_F is the fitted melt at each cell, μ_F is the spatial average of M_F, and σ_F is the spatial SD of M_F. From the relative distribution of melt, we use the mean melt water quantities μ_J from an ice sheet model of Thwaites Glacier (13) that include frictional melting, horizontal advection, and an assumed uniform geothermal flux of 70 mW/m^2 to scale our results so that the total radar inferred quantity is equal to the total modeled melt water quantity for the upstream region of the Thwaites Glacier. We also scaled the standard deviation of the radar inferred melt water by the spatial standard deviation of routed subglacial water σ_Q using the same total melt (13). The resulting radar inferred melt water quantity M is given by

$$M = Z_F \sigma_Q \left(\frac{\mu_J}{\mu_Q}\right) + \mu_J.$$

Inferred Geothermal Flux. From this inferred melt, we subtracted the mean value for the net modeled frictional and advective contributions to basal melt (13) and calculate the geothermal flux G required to produce the remaining melt given by

$$G = (M - \mu_J)L_w + 70 \ \ mW/m^2,$$

where L_w is the latent heat of fusion of water and 70 mW/m^2 is the uniform geothermal heat flux used in the ice sheet model (13). We estimate the notional uncertainty on the inferred geothermal flux (ΔG) to be given by

$$\Delta G = \sigma_Q \left(\frac{\mu_J}{\mu_Q}\right) L_w.$$

1. Schroeder DM, Blankenship DD, Young DA (2013) Evidence for a water system transition beneath Thwaites Glacier, West Antarctica. *Proc Natl Acad Sci USA* 110(30):12225–12228.
2. Walder JS, Fowler A (1994) Channelized subglacial drainage over a deformable bed. *J Glaciol* 40(134):3–15.
3. Knott EF, Shaeffer JF, Tuley MT (2004) *Radar Cross Section* (SciTech, Raleigh, NC).
4. Peters ME, Blankenship DD, Morse DL (2005) Analysis techniques for coherent airborne radar sounding: Application to West Antarctic ice streams. *J Geophys Res* 110(B6):B06303.
5. MacGregor JA, et al. (2007) Modeling englacial radar attenuation at Siple Dome, West Antarctica, using ice chemistry and temperature data. *J Geophys Res* 112(F3):F03008.
6. Matsuoka K (2011) Pitfalls in radar diagnosis of ice-sheet bed conditions: Lessons from englacial attenuation models. *Geophys Res Lett* 38(5):L05505.
7. Gades AM, Raymond CF, Conway H, Jacobel RW (2000) Bed properties of Siple Dome and adjacent ice streams, West Antarctica, inferred from radio-echo sounding measurements. *J Glaciol* 46(152):88–94.
8. Von Storch H, Zwiers FW (2001) *Statistical Analysis in Climate Research* (Cambridge Univ Press, Cambridge, UK).
9. Le Brocq AM, Payne AJ, Siegert MJ, Alley RB (2009) A subglacial water-flow model for West Antarctica. *J Glaciol* 55(193):879–888.
10. Fretwell P, et al. (2013) Bedmap2: Improved ice bed, surface and thickness datasets for Antarctica. *Cryosphere* 7:375–393.
11. Holmgren P (1994) Multiple flow direction algorithms for runoff modeling in grid based elevation models: An empirical evaluation. *Hydrol Processes* 8(4):327–334.
12. Menke W (2012) *Geophysical Data Analysis: Discrete Inverse Theory* (Academic, New York).
13. Joughin IR, et al. (2009) Basal conditions for Pine Island and Thwaites Glaciers, West Antarctica, determined using satellite and airborne data. *J Glaciol* 55(190): 245–257.

Other Supporting Information Files

Dataset S1 (TXT)